Online Parameterization of Lumped Thermal Dynamics in Cylindrical Lithium Ion Batteries for Core Temperature Estimation and Health Monitoring

Xinfan Lin, Hector E. Perez, Jason B. Siegel, Anna G. Stefanopoulou, *Fellow, IEEE*, Yonghua Li, R. Dyche Anderson, Yi Ding, and Matthew P. Castanier

***Abstract*— Lithium ion batteries should always be prevented from overheating and, hence, thermal monitoring is indispensable. Since only the surface temperature of the battery can be measured, a thermal model is needed to estimate the core temperature of the battery, which can be higher and more critical. In this paper, an online parameter identification scheme is designed for a cylindrical lithium ion battery. An adaptive observer of the core temperature is then designed based on the online parameterization methodology and the surface temperature measurement. A battery thermal model with constant internal resistance is explored first. The identification algorithm and the adaptive observer is validated with experiments on a $2.3Ah$ 26650 lithium iron phosphate/graphite battery. The methodology is later extended to address temperature-dependent internal resistance with nonuniform forgetting factors. The ability of the methodology to track the long-term variation of the internal resistance is beneficial for battery health monitoring.**

***Index Terms*— Adaptive estimation, core temperature, lithium ion battery, state of health.**

I. Introduction

LITHIUM ion batteries have been widely considered as an energy storage device for hybrid electric vehicles (HEV), plug-in hybrid electric vehicles (PHEV), and battery electric vehicles (BEV). Thermal management in vehicular applications is a critical issue for lithium ion batteries because of their narrow operating temperature range. An accurate prediction of battery temperature is key to maintaining the safety, performance, and longevity of these Li-ion batteries.

Manuscript received March 6, 2012; revised August 6, 2012; accepted August 17, 2012. Manuscript received in final form August 29, 2012. Recommended by Associate Editor S. Varigonda.

X. Lin, H. E. Perez, J. B. Siegel, and A. G. Stefanopoulou are with the Department of Mechanical Engineering, University of Michigan, Ann Arbor, MI 48109 USA (e-mail: xflin@umich.edu; heperez@umich.edu; siegeljb@umich.edu; annastef@umich.edu).

Y. Li and R. D. Anderson are with the Vehicle and Battery Controls Department, Research and Advanced Engineering, Ford Motor Company, Dearborn, MI 48121 USA (e-mail: yli19@ford.com; rander34@ford.com).

Y. Ding and M. P. Castanier are with the U.S. Army Tank Automotive Research, Development, and Engineering Center (TARDEC), Warren, MI 48397 USA (e-mail: yi.ding8.civ@mail.mil; matthew.p.castanier.civ@mail.mil).

Color versions of one or more of the figures in this paper are available online at http://ieeexplore.ieee.org.

Digital Object Identifier 10.1109/TCST.2012.2217143

Existing high fidelity thermal models can predict the detailed temperature distribution throughout the cell [1]–[4]. However, these models are not suitable for onboard application due to their high computational intensity. Reduced order models typically use one single temperature, the bulk (or average) temperature, to capture the lumped thermal dynamics of the cell [4]–[7]. Even though the single temperature approximation is computationally efficient, it might lead to over-simplification since the temperature in the battery core can be much higher than in the surface [8].

Lumped thermal models capturing both the surface and the core temperatures of the cell have also been studied in [8] and [9]. Such simplified models are efficient for onboard application due to their limited number of states. The accuracy of the model parameters is of great importance since it determines the accuracy of the core temperature estimation. Model parameters can be approximated based on the geometry of the battery and the volume averaging physical properties of its components [9], but such approximation may not be accurate due to the complicated layered structure of the cell and the interfaces between the layers. The parameters can also be determined by fitting the model to the data obtained from experiments [8], involving designed input excitation and measurement of the battery core temperature. This laboratory-oriented parameterization is invaluable for determining the initial values of parameters. However, some of the parameters, such as the internal resistance, may change over the battery lifetime due to degradation. In this case, parameter mismatch leads to inaccurate temperature estimation, and thus identification of present value of the parameters is needed.

A recursive parameter identification scheme is designed, in this paper, to automatically identify the thermal model parameters based on the signals commonly measured in a vehicle battery management system (BMS). The algorithm is simple enough to run on a typical automotive onboard controller. An adaptive observer is then designed for the core temperature estimation. A lumped battery model with constant internal resistance is investigated first, where the least square algorithm is sufficient for identification. In reality, the internal resistance of the battery can be temperature and/or state of charge (SoC)-dependent [5], [10], [11] and hence time-varying. The pure least square algorithm may cause errors

in the identification if the actual parameters are nonconstant. Nonuniform forgetting factors are augmented to the least square algorithm to address the issue of time-varying internal resistance.

Apart from the short-term variability due to conditions, such as temperature, the internal resistance of the lithium ion battery may also increase over its lifetime due to degradation. This is because the solid electrolyte interphase (SEI) may grow in thickness [12]–[14] and reduce the conductivity of the SEI. Hence, the least square algorithm with nonuniform forgetting factors is also applied to track the long-term growth of the internal resistance. The growth of the internal resistance can be viewed as an important indication of the state of health (SOH) of the battery, and used as a reference for the onboard BMS to extend the life of the batteries. Parameterization of battery model and adaptive monitoring of the battery voltage and SOH have been explored previously in various seminal papers [15]–[17], but this paper is among the first to adaptively monitor the temperatures (especially the core temperature) of batteries and SOH from a thermal perspective.

II. Lumped Thermal Model of a Cylindrical Lithium Ion Battery

The radial thermal dynamics of a cylindrical battery are modeled based on the classic heat transfer problem by assuming heat generation located at the core and zero heat flux at the center, as shown in Fig. 1.

The two-state approximation of the radially distributed thermal model is defined as [9]

$$C_c \dot{T}_c = I^2 R_e + \frac{T_s - T_c}{R_c} \tag{1a}$$

$$C_s \dot{T}_s = \frac{T_f - T_s}{R_u} - \frac{T_s - T_c}{R_c} \tag{1b}$$

where the two states are the surface temperature T_s and the core temperature T_c. The temperature variation along the battery height is neglected here, assuming homogeneous conditions.

Heat generation is approximated as a concentrated source of Joule loss in the battery core, computed as the product of the current I squared and the internal resistance R_e. The internal resistance R_e is considered as an unknown parameter to be identified. This simplification can lead to cycle-dependent values for lumped resistance R_e, or even nonconstant resistance within a single cycle, because R_e can vary with conditions, such as temperature, SoC and degradation [5], [10], [11], [13]. In subsequent sections, first, R_e will be identified online as a constant under a drive cycle, and then identification of R_e as a varying parameter will be addressed in Section VII. Heat generation calculated based on an equivalent circuit model has also been used for thermal model parameterization in another ongoing work [18].

Heat exchange between the core and the surface is modeled by heat conduction over a thermal resistance, R_c which is a lumped parameter aggregating the conduction and contact thermal resistance across the compact and inhomogeneous materials. A convection resistance R_u is modeled between the surface and the surrounding coolant to account for convective cooling. The value of R_u is a function of the coolant flow rate, and in some vehicle battery systems, the coolant flow rate is adjustable to control the battery temperature. Here, it is modeled as a constant as if the coolant flow rate is fixed to accommodate the maximum required cooling capacity. A model with the more complicated varying R_u has also been investigated in [19].

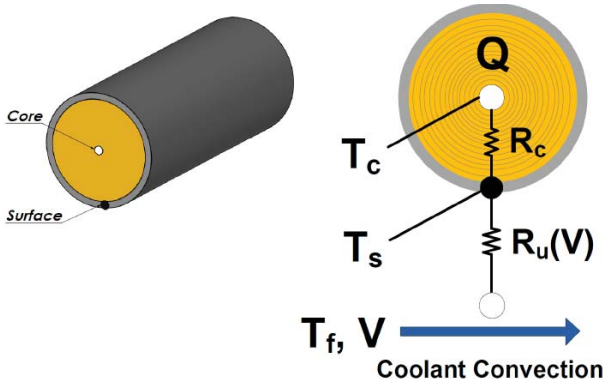

Fig. 1. Single cell radially lumped thermal model.

The rates of temperature change of the surface and the core depend on their respective lumped heat capacity. The parameter C_c is the heat capacity of the jelly roll inside the cell, and C_s is related to the heat capacity of the battery casing.

The complete parameter set for this model includes C_c, C_s, R_e, R_c, and R_u, of which the values cannot be easily calculated. Consider the conduction resistance R_c as an example. Theoretically, R_c can be calculated based on the conductivity and dimensions of the wound cell electrode assembly and the aluminum casing. However, since the rolled electrodes are composed by the cathode, anode, current collectors, and separator, it will be difficult to obtain an accurate value for the overall conductivity. Moreover, R_c also includes the contact thermal resistance between the rolled electrodes and the casing, which involves various contact properties adding to the complexity of the calculation.

Therefore, model identification techniques are developed in the following section to obtain the lumped phenomenological values of the model parameters based on measurable inputs and outputs of the model.

III. Parameterization Methodology

For model identification, a parametric model

$$z = \theta^T \phi \tag{2}$$

is derived first by applying Laplace transformation to the model, where z is the observation, θ is the parameter vector, and ϕ is the regressor [20]. Both z and ϕ should be measured or can be generated from measured signals.

With a parametric model, various algorithms can be chosen for parameter identification, such as the gradient and the least squares methods. The method of least squares is preferred for noise reduction [20].

The recursive least squares algorithm is applied in an online fashion, as parameters are updated continuously [20]

$$\dot{\theta} = P\frac{\epsilon\phi}{m^2} \tag{3a}$$

$$\dot{P} = -P\frac{\phi\phi^T}{m^2}P \tag{3b}$$

$$\epsilon = z - \theta^T\phi \tag{3c}$$

$$m^2 = 1 + \phi^T\phi \tag{3d}$$

where m is a normalization factor that enhances the robustness of parameter identification.

In some cases, to make the observation z and the regressors ϕ proper (or causal), a filter $(1/\Lambda(s))$ will have to be designed and applied. The parametric model will then become

$$\frac{z}{\Lambda} = \theta^T\frac{\phi}{\Lambda}. \tag{4}$$

The convergence and robustness of the identification are guaranteed if the regressors, ϕ in (8), are stationary signals and satisfy the persistent excitation (PE) conditions [20]. The PE conditions are satisfied if there exist some time interval T_0, and positive number α_1 and α_0, such that

$$\alpha_1 I_M \geq U(t) = \frac{1}{T_0}\int_t^{t+T_0}\phi(\tau)\phi^T(\tau)d\tau \geq \alpha_0 I_M \qquad \forall t \geq 0 \tag{5}$$

where I_M is the identity matrix with the same dimension as $U(t)$ [20]. This criteria can be used to test whether a drive cycle can ensure robust parameter convergence.

IV. Online Parameterization of the Battery Thermal Model

In this section, the parameterization scheme described previously is applied to the cylindrical battery thermal model in (1). A parametric model for identification can be derived by taking the Laplace transformation of (1) and replacing the unmeasured T_c with measured signals I, T_f, and T_s

$$\begin{aligned} s^2T_s - sT_{s,0} = {} & \frac{R_e}{C_cC_sR_c}I^2 + \frac{1}{C_cC_sR_cR_u}(T_f - T_s) \\ & + \frac{1}{C_sR_u}s(T_f - T_s) - \frac{1}{C_cC_sR_c} \\ & \times\big((C_c + C_s)sT_s - C_sT_{s,0} - C_cT_{c,0}\big) \end{aligned} \tag{6}$$

where $T_{s,0}$ and $T_{c,0}$ are the initial surface and core temperatures. When the initial core temperature, $T_{c,0}$, is considered to be the same as the initial surface temperature, $T_{s,0}$, as if the battery starts from thermal equilibrium, (6) becomes

$$\begin{aligned} s^2T_s - sT_{s,0} = {} & \frac{R_e}{C_cC_sR_c}I^2 + \frac{1}{C_cC_sR_cR_u}(T_f - T_s) \\ & - \frac{C_c+C_s}{C_cC_sR_c}(sT_s - T_{s,0}) + \frac{1}{C_sR_u}s(T_f - T_s). \end{aligned} \tag{7}$$

It is assumed here that T_f is regulated as a steady output of the air-conditioning unit and thus $sT_f = 0$, giving

$$\begin{aligned} s^2T_s - sT_{s,0} = {} & \frac{R_e}{C_cC_sR_c}I^2 + \frac{1}{C_cC_sR_cR_u}(T_f - T_s) \\ & - \left(\frac{C_c + C_s}{C_cC_sR_c} + \frac{1}{C_sR_u}\right)(sT_s - T_{s,0}). \end{aligned} \tag{8}$$

If T_f is a time-varying input to the model, sT_f should not be dropped. In this case, T_f can also be used as an input excitation in the parametric model. A second order filter should be applied to the observation and the regressors in (8) to make them proper. The filter takes the form

$$\frac{1}{\Lambda(s)} = \frac{1}{(s + \lambda_1)(s + \lambda_2)} \tag{9}$$

where λ_1 and λ_2 are the time constants of the filter. The values of λ_1 and λ_2 can be chosen to filter the noises with frequencies higher than the temperature dynamics.

For the parametric model in (8)

$$Z(s) = \frac{s^2T_s - sT_{s,0}}{\Lambda(s)} \tag{10a}$$

$$\Phi(s) = \begin{bmatrix} \dfrac{I^2}{\Lambda(s)} & \dfrac{T_f - T_s}{\Lambda(s)} & \dfrac{sT_s - T_{s,0}}{\Lambda(s)} \end{bmatrix}^T \tag{10b}$$

$$\theta = [\alpha \quad \beta \quad \gamma\,]^T \tag{10c}$$

where

$$\alpha = \frac{R_e}{C_cC_sR_c} \tag{11a}$$

$$\beta = \frac{1}{C_cC_sR_cR_u} \tag{11b}$$

$$\gamma = -\left(\frac{C_c + C_s}{C_cC_sR_c} + \frac{1}{C_sR_u}\right). \tag{11c}$$

For implementation in a practical system, the identification algorithm is formulated along with signals z and ϕ in the time domain based on (3), or in the discrete time domain based on equivalent formula. For example, $z(t)$, whose Laplace transform is $(s^2T_s - sT_{s,0}/\Lambda(s))$, can be obtained by calculating the convolution of $T_s(t) - T_{s,0}$ and the inverse Laplace transform of $(s^2/\Lambda(s))$. In this way, calculation of the second order derivative of T_s, s^2T_s, which can be easily corrupted by noises, is avoided.

By using the parametric model in (8), only three lumped parameters, α, β, and γ, can be identified under the condition of persistent input excitation [20]. Prior knowledge of two of the physical parameters must be assumed so as to determine a set of unique solutions for the original five physical parameters, Cc, Cs, Re, Rc, and Ru from α, β, and γ. Of the five physical parameters, the internal resistance R_e may vary due to aging and should be identified online. The conduction resistance R_c is difficult to estimate as explained previously. The convection resistance R_u will be influenced by the coolant flow conditions around the cell depending on the packaging. Therefore, it is not easy to obtain prior knowledge of those three parameters. The heat capacities C_c and C_s, which depend on the thermal properties and the mass of the rolled electrode assembly and the casing, are relatively constant over lifetime. In addition, the heat capacities will only affect the speed of transient response of the model without having any impact on the steady state temperatures. Consequently, the heat capacities C_c and C_s are selected to be the presumed parameters.

With C_c and C_s presumed and α, β, and γ identified, R_e, R_c, and R_u can be obtained by solving the following set

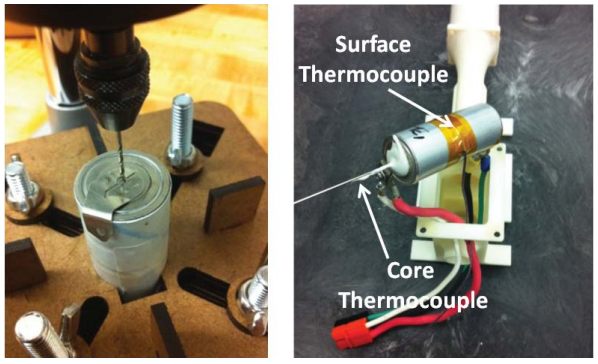

Fig. 2. Instrumentation of the battery core temperature. (a) Drill press setup of the battery. (b) Installation of the thermocouples.

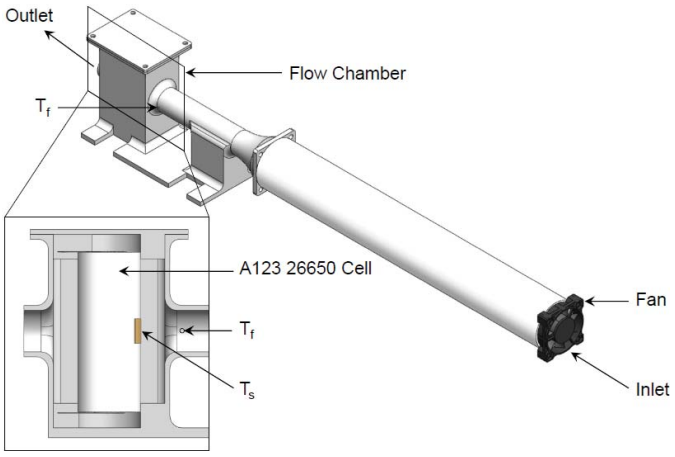

Fig. 3. Schematic diagram of the flow chamber.

of equations:

$$\beta(C_c + C_s)C_s {R_u}^2 + \gamma\, C_s R_u + 1 = 0 \tag{12a}$$

$$R_c = \frac{1}{\beta C_s C_c R_u} \tag{12b}$$

$$R_e = \alpha C_c C_s R_c. \tag{12c}$$

The quadratic equation for R_u in (12) can lead to two solutions, but the right one can be decided based on the coolant flow conditions based on [21].

The least squares algorithm in (3) can then be applied for parameter identification. In [19] and [22], the methodology has been applied and verified by simulation with a battery thermal model with assumed parameters. In the following section, the parameterization is further validated by experiments.

V. Experiment Validation

A. Experiment Set-Up and Measurements

Experiments have been conducted to validate the designed parameterization scheme. A 2.3Ah *A*123 26650 $LiFePO_4$/graphite battery is cycled with a Bitrode cycler under the control of a customized testing system by A&D Technology. A Cincinnati Sub-Zero environmental simulation chamber is used to regulate the temperature of the coolant air flow around the battery.

T-type thermocouples are installed both on the battery casing to measure its surface temperature, and also inside the battery core to measure the core temperature. During the fabrication process of the 26 650 cylindrical cell, the electrode assembly is wound up to form a roll, leaving a cavity in the center. To measure the core temperature, the battery was drilled inside an argon-filled glove box through to its central cavity, where the thermocouple was inserted, as shown in Fig. 2. The battery was then sealed and taken out of the glove box for experiments.

Inside the thermal chamber, the battery was placed in a designed flow chamber as shown in Fig. 3, where a fan was mounted at one end to regulate the air flow around the cell. The speed of the fan is controlled by pulse width modulation signals to change the air flow rate. The flow chamber is used to emulate the pack air cooling conditions where the coolant flow rate is adjustable (like in [19]). A T-type thermocouple is placed near the battery inside the flow chamber to measure the air flow temperature T_f.

B. PE of Input Signals

A driving cycle, the urban assault cycle (UAC) [23], is applied as the current excitation to the battery in galvanostatic mode. The UAC was originally a velocity cycle for military vehicles. The current profile for a battery pack of a hybrid military vehicle under UAC was derived in [23] by applying a certain power management strategy. The type of battery used in the experiment ($LiFePO_4$ 26650) is different from the one in [23], hence the UAC current cycle taken from [23] is rescaled for the experiments. The original 20-minute cycle is repeated 4 times to let the battery temperature reach periodic steady state. The resulting scaled drive cycle current is plotted in Fig. 4. The normalized unit of C-rate is commonly used to describe the load applied to the battery and 1 C corresponds to the magnitude of the current that depletes the battery in one hour (in this case 2.3 A). The negative current indicates the discharge of the battery as the energy is drawn from the battery to drive the vehicle, and the positive current represents the regenerative braking during which the battery is charged. The discharge load is fairly evenly distributed between 1 C and 7 C, except at around -8 C which indicates rapid acceleration. The charge load is mostly below 7 C and occasionally reaches above 10 C during drastic braking. The SoC evolution under this cycle is also plotted in Fig. 4, showing a decrease from about 50% to roughly 35%.

The temperature of the thermal chamber is controlled at 26 °C. The resulting battery surface temperature T_s and air flow temperature T_f are measured and recorded by the data acquisition system. The measured T_s and T_f under the scaled UAC cycles are plotted in Fig. 5, which along with I are then used for parameter identification.

The criteria in (5) is then applied to check if the UAC cycle satisfies the PE condition, which requires the regressors to be stationary signals first. As can be seen in Fig. 5, the surface temperature T_s will vary periodically after the battery finishes the warm-up phase at about 1000 s. Consequently, the regressors, which include I^2, $T_f - T_s$, and sT_s, will become

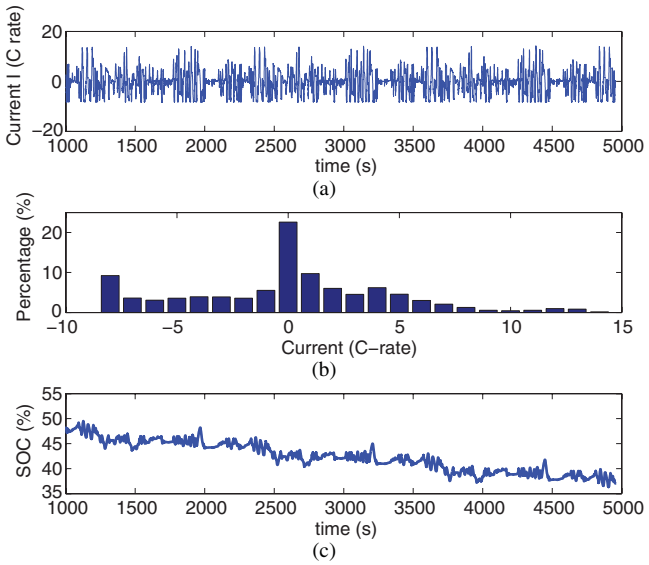

Fig. 4. Scaled UAC current excitation. (a) Currents in time series. (b) Histogram of the currents. (c) SoC variation under the cycle.

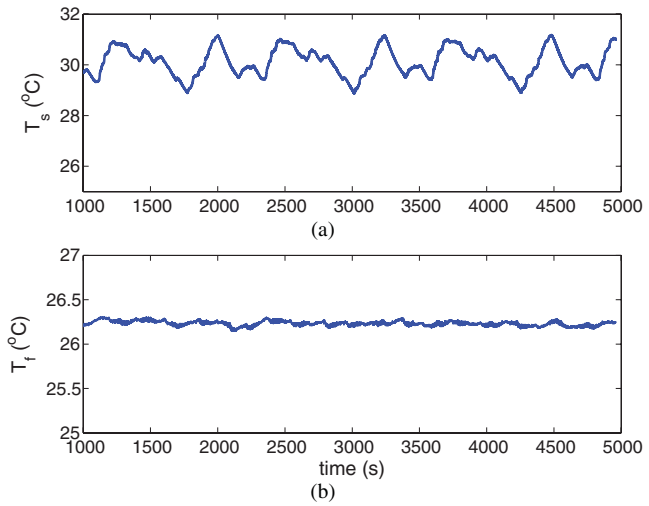

Fig. 5. Measured T_s and T_f under scaled UAC cycle. (a) Surface temperature T_s. (b) Flow temperature T_f.

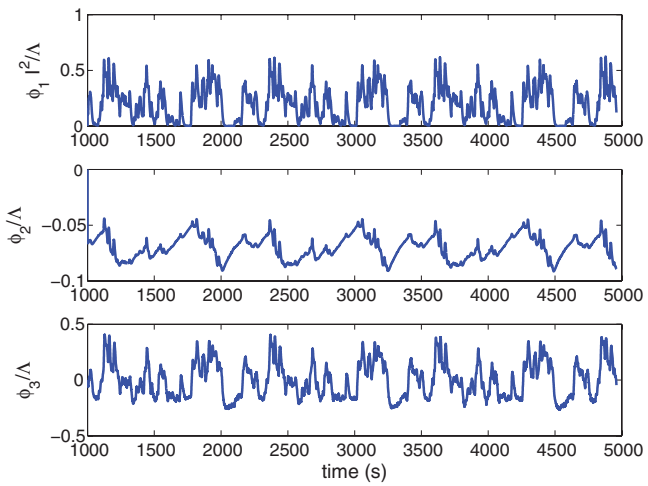

Fig. 6. Evolution of regressors ϕ in periodic steady state.

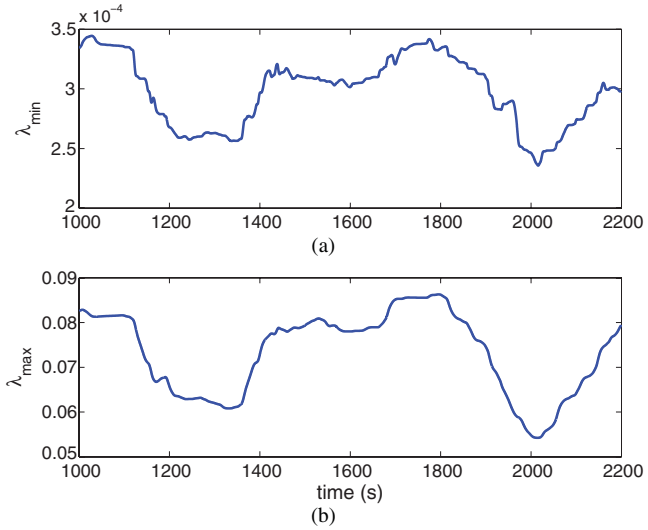

Fig. 7. Evolution of the eigenvalues of $U(t)$ in steady state. (a) Smallest eigenvalue. (b) Largest eigenvalue.

stationary signals, as shown in Fig. 6. The $U(t)$ matrix can then be calculated to check the PE conditions. It is noted that the measurements taken during the warm-up period can also be used for identification, even though they are not stationary signals [19].

Since the current input consists of repeated UAC cycles (each lasting for 1200 s), the values of $U(t)$ only need to be calculated over a time interval $T_0 = 1200$ s for 1000 s $\leq t \leq$ 2200 s. It is noted that in this case, $U(t)$ is not a diagonal matrix, and thus its eigenvalues are calculated to check the PE conditions. The smallest and the largest eigenvalues of $U(t)$, $\lambda_{\max}$, and $\lambda_{\min}$, are plotted in Fig. 7. It can be concluded from Fig. 7 that α_1 in (5) can be found as 0.086 s^{-1}, which is the maximum of $\lambda_{\max}(t)$, and α_0 as 2.4×10^{-4} s^{-1}, which is the minimum of $\lambda_{\min}(t)$. Consequently, under the UAC cycle, the regressors satisfy the conditions of PE. Furthermore, α_0 are related to the speed of the convergence for parameter identification. Specifically, when the gradient method is used, $2\alpha_0^{-1}$ is the upper limits of the time constant of the parameter convergence [20], which would be

$$\tau \leq 8333 \text{ s} \tag{13}$$

in this case. Based on (13), the 90% settling time for the convergence under the gradient search algorithm is expected to be less than 19186 s. It is noted that 19186 s is a rather conservative estimation of the convergence time. In real applications, the convergence is usually accelerated by increasing the adaptive gain [20], [24].

C. Results and Discussion

The measured signals I, T_s, and T_f in Figs. 4 and 5 are used for recursive least squares parameterization. The three parameters to be identified, R_u, R_e, and R_c, are initialized with the initial guess values in Table I. For the heat capacity, the single C_p in [8] is split into C_c and C_s here representing the battery core and surface heat capacities, respectively. The heat

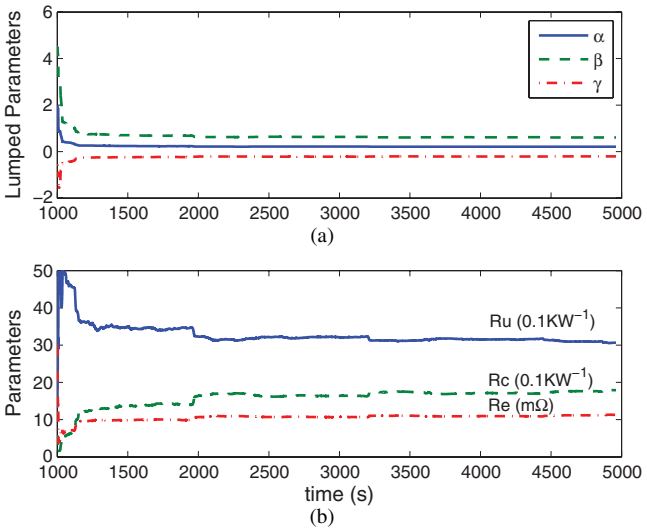

Fig. 8. Online parameter identification results. (a) Convergence of the lumped parameters. (b) Convergence of the original parameters.

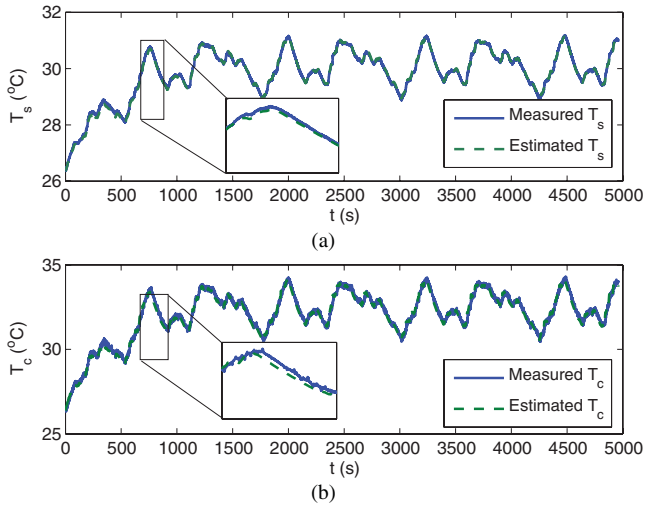

Fig. 9. Experimental validation. (a) Estimated surface temperature T_s versus measured. (b) Estimated core temperature T_c versus measured.

TABLE I
INITIAL GUESS AND IDENTIFICATION RESULTS OF PARAMETERS

Parameters	R_u(KW^{-1})	R_e(mΩ)	R_c(KW^{-1})
Initial Guess	1.5	30	0.5
ID Results	3.03	11.4	1.83

TABLE II
COMPARISON OF THE IDENTIFIED PARAMETERS TO [8]

Parameters	Value	Equivalence in [8]	Value
R_c(KW^{-1})	1.83	R_{in}(KW^{-1})	3.2 ∼ 3.4
R_u(KW^{-1})	3.03	R_{out}(KW^{-1})	8.4 ∼ 9.1
C_c(JK^{-1})	67	C_p(JK^{-1})	73 ∼ 78
C_s(JK^{-1})	4.5	-	-

capacity of the battery core, C_c, is assumed to be 67 JK^{-1}, slightly smaller than C_p in [8]. The heat capacity of the battery surface, C_s, is assumed to be 4.5 JK^{-1} based on the dimensions of the aluminum casing of the 26 650 battery and the specific heat capacity of aluminum.

The results of the recursive identification are plotted in Fig. 8. It is noted that the identification procedures are started after the first 1000 s when the temperature enters periodic steady state. It can be seen that starting at some random initial values, the three parameters converge to the values listed in Table I. Fig. 8(a) shows the convergence of the lumped parameters α, β, and γ in (8), and Fig. 8(b) shows the convergence of the physical parameters R_u, R_c, and R_e, which are obtained by solving (12). It is noted that the convergence time is within the range (less than 19 186 s) discussed in Section V-B, which is strictly speaking only valid for the gradient method. The convergence rate is accelerated here by increasing the initial adaptive gain P_0 [24], [25], which is the initial value of $P(t)$ in (3).

For validation purposes, the identified parameters are applied to (1) to estimate both the battery surface temperature T_s and the core temperature T_c. The estimate is then compared with the measurement, as plotted in Fig. 9. The estimated surface temperatures T_s match the measurement exactly, since T_s is directly used for identification. It is noted that the measured core temperature T_c also agrees closely with the measured T_c (which was not used for parameterization), showing the capability of the parameterized model to predict the correct battery core temperatures. Once the parameterization scheme is validated, it can be run in onboard BMS to estimate the core temperatures in real time without actually measuring it (as in the lab set-up).

The identification results are also compared to those in [8], where thermal parameters of the same battery are identified based on the measurement of both surface and core temperatures under designed current inputs. In [8], the battery is modeled with a single dynamic state (the core temperature), and the surface temperature is related to the core temperature with an algebraic equation by assuming the surface heat capacity to be zero. In [8], the heat generation is pre-calculated by resistive heat dissipation (due to ohmic voltage drop) plus entropic heat, and in this paper, the entropic heat is ignored and the heat generation is accounted for by multiplying the current square with an identified parameter R_e. It is noted that the entropic heat is generally small comparing to the resistive heat, especially in the middle SoC range here as shown in Fig. 4.

Table II summarizes the comparison between the thermal parameters identified in [8] and in this paper. It can be seen that the identified value of the conduction resistance (R_c) between the core and the surface is smaller than that in [8]. This is probably because the surface temperature in this paper is measured at the aluminum casing instead of at the outside paper cover (as in [8]), which indicates better heat conduction. The identified convection resistance between the surface and the coolant R_u is significantly smaller than that in [8], which can be explained by the fact that during the experiment, the air flow is constantly blown into the flow chamber by the fan, which enhances the convective cooling through the coolant air.

VI. Adaptive Battery Core Temperature Estimation

In controlled applications, an observer is often designed based on a plant model to estimate the states of a plant, especially ones that are not measured, e.g., the core temperature T_c of the battery in this case. Such model-based observers can be categorized as either an open-loop observer or a closed-loop observer. For a linear system

$$\dot{x} = Ax + Bu \tag{14}$$

where x are the states and u are the inputs, an open-loop observer is simply

$$\dot{\hat{x}} = A\hat{x} + Bu \tag{15}$$

as the estimated states $\hat{x}$ are calculated by the model solely based on the inputs u. For the battery thermal model specifically, we have

$$x = [T_c \quad T_s]^T \tag{16a}$$

$$u = [I^2 \quad T_f]^T \tag{16b}$$

$$A = \begin{bmatrix} -\frac{1}{R_c C_c} & \frac{1}{R_c C_c} \\ \frac{1}{R_c C_s} & -\frac{1}{C_s}\left(\frac{1}{R_c} + \frac{1}{R_u}\right) \end{bmatrix} \tag{16c}$$

$$B = \begin{bmatrix} \frac{R_e R_c}{C_c} & 0 \\ 0 & \frac{1}{R_u C_s} \end{bmatrix}. \tag{16d}$$

However, the estimation by such an open-loop observer can often be corrupted by unknown initial conditions, and noises in the measurement of the inputs. To address such issues, a closed-loop observer, such as a Luenberger observer or a Kalman filter, is often designed to estimate the states based on the model and the feedback of some measurable outputs [26]

$$\dot{\hat{x}} = A\hat{x} + Bu + L(y - \hat{y}) \tag{17a}$$

$$y = Cx + Du \tag{17b}$$

$$\hat{y} = C\hat{x} + Du \tag{17c}$$

where y are the measured system outputs, $\hat{x}$ and $\hat{y}$ are estimated states and output, L is the observer gain, and A, B, C, and D are model parameters. For the battery thermal model, since the surface temperature T_s is measurable, we have

$$C = [0 \quad 1] \tag{18a}$$

$$D = 0. \tag{18b}$$

It is noted that the difference between the measured and the estimated output is used as the feedback to correct the estimated states. Comparing with an open-loop observer, the closed-loop observer can accelerate the convergence of the estimated states to those of the real plant under unknown initial conditions, e.g., a Luenberger observer [26], or optimize the estimation by balancing the effect of unknown initial conditions and noises, e.g., a Kalman filter [27].

By taking the structure of a closed-loop observer, an adaptive observer is then designed based on the certainty equivalence principle [20]

$$C_c \dot{\hat{T}}_c = I^2 \hat{R}_e + \frac{\hat{T}_s - \hat{T}_c}{\hat{R}_c} + l_1(T_s - \hat{T}_s) \tag{19a}$$

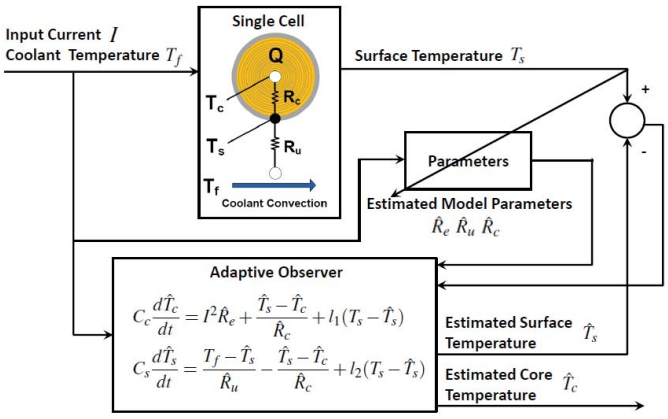

Fig. 10. Online identification scheme and adaptive observer structure.

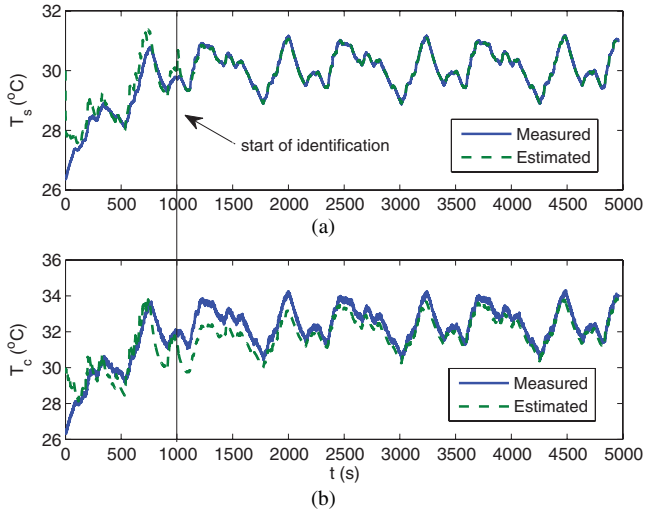

Fig. 11. Response of the closed-loop adaptive observer. (a) Adaptive estimation of the surface temperature versus measurement. (b) Adaptive estimation of the core temperature versus measurement.

$$C_s \dot{\hat{T}}_s = \frac{T_f - \hat{T}_s}{\hat{R}_u} - \frac{\hat{T}_s - \hat{T}_c}{\hat{R}_c} + l_2(T_s - \hat{T}_s) \tag{19b}$$

where $\hat{T}_s$ and $\hat{T}_c$ are the estimated surface and core temperatures, and the observer parameters $\hat{R}_e$, $\hat{R}_c$, and $\hat{R}_u$ are taken from the online identification results in Section V. The block diagram of the adaptive observer is shown in Fig. 10. The input current I, coolant temperature T_f, and the measured surface cell temperature T_s are fed into the parameter identifier to estimate model parameters R_u, R_e, and R_c. The adaptive observer uses the estimated parameters to estimate the core and the surface temperatures. The estimated T_s is compared to the measurement and the error is fed back to correct the core temperature and surface temperature estimation. The estimations for both parameters and temperatures are updated at each time step.

The data in Section V are used to test the response of the adaptive observer, as plotted in Fig. 11. The initial estimated temperatures of the adaptive observer are set at 30 °C for both the surface and the core, whereas the correct value is 26 °C, and the parameters are initialized with the initial guess values in Table I. It can be seen from Fig. 11 that the estimated

surface temperature T_s converges to the actual values much faster than the core temperature T_c. The reason is that the surface temperature T_s is accessible by the adaptive observer both via parameter identification and closed-loop error feedback, and thus the observer can adjust its estimation of T_s quickly based on direct reference of the measurement. But for the core temperature T_c, which is not measured, its estimation accuracy depends on the accuracy of the model parameters. Therefore, the convergence of T_c to the actual values will only happen after the identified parameters converge to the correct model parameters (at approximately 3000 s).

VII. Parameterization of the Battery Thermal Model With Temperature-Dependent R_e

For most lithium ion batteries, their internal resistance R_e depends on temperature and SoC, [5], [6], [11]. In general cases, R_e is high when the temperatures are low and when the SoC is close to 0% or 100%. An Arrhenius function is often used to describe the relationship between R_e and the battery (core) temperature T_c, as

$$R_e = R_{e,\text{ref}} \exp\left(\frac{T_{\text{ref}}}{T_c}\right) \tag{20}$$

where $R_{e,\text{ref}}$ is the reference resistance value at a certain reference temperature T_{ref}, and T_{ref} and T_c are in K. It is noted that the change in resistance with respect to SoC is negligible in the normal vehicle battery operating range (20%−80% SoC) and thus is not considered here. The relationship between R_e and T_s described by (20) is plotted in Fig. 12, by taking $R_{e,\text{ref}} = 0.091$ mΩ and $T_{\text{ref}} = 1543$ K.

As a result, in real application, R_e will be varying as the temperature fluctuates. Such variation cannot be neglected when the power demands are high and dramatically varying. Simulation is used in this section for illustration. Simulated variation of R_e due to T_c fluctuation under a drastic current cycle is shown in Fig. 13. It can be seen that the drastic current variation creates a 10 °C of fluctuation in the battery core temperature T_c. The resulting variation of R_e is about 20% as shown by the blue line in the bottom plot of Fig. 13.

Since the least squares identification algorithm in (3) identifies each parameter as a constant, when R_e is varying, errors will be observed in R_e identification as shown in Fig. 13. This will not only introduce errors in R_e estimation but might also affect the estimation of other parameters, and eventually corrupt the estimation of the core temperature T_c. To address such issue, a least squares algorithm with forgetting factors is then designed to identify R_e as a time-varying parameter.

A. Identification Design With Forgetting Factor

When forgetting factors are adopted, most parts of the least square algorithm will be the same as (3), except that

$$\dot{P}(t) = \eta^T P(t)\eta - P(t)\frac{\phi(t)\phi^T(t)}{m^2(t)}P(t) \tag{21}$$

where η is the forgetting factor matrix [20].

The least square identification algorithm tries to find the optimal parameters that best fit the inputs and outputs over the whole data set. A pure least square algorithm treats each data point as equal, no matter if it is acquired most recently, or obtained much earlier. However, when a forgetting factor is applied, the data points will be weighted differently. Specifically, the newly acquired data are favored over the older ones. In the form shown in (21), the weight of the data will decay exponentially with the time elapsed, and the larger the forgetting factor is, the faster the decay will be. Consequently, the least square algorithm can track the parameters when they are time-varying.

The least square algorithm with forgetting factors can be applied to the original linear parametric model in (7). Of the three lumped parameters, namely α, β, and γ in (7), only α is related to time varying R_e, and all the others are constant. Therefore, nonuniform forgetting factors should be adopted with the η matrix designed as

$$\eta = \begin{bmatrix} \eta_1 & 0 & 0 \\ 0 & 0 & 0 \\ 0 & 0 & 0 \end{bmatrix} \tag{22}$$

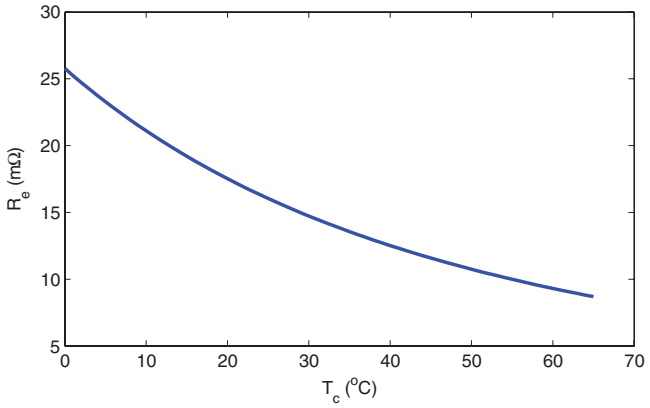

Fig. 12. Dependence of R_e on T_c.

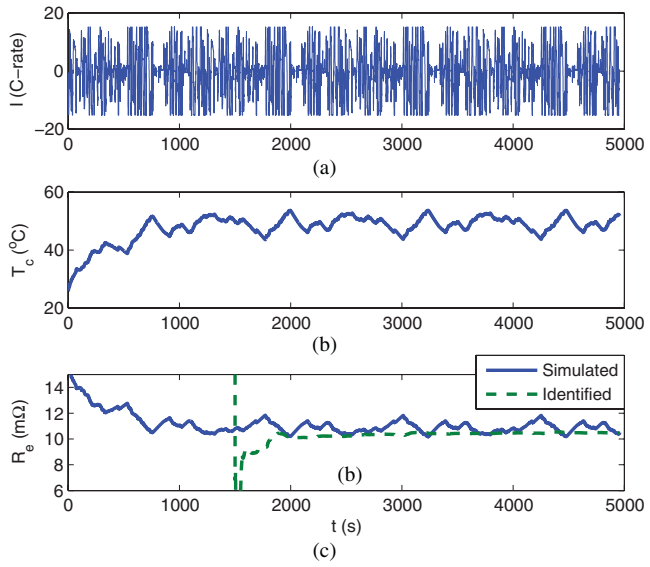

Fig. 13. Errors in R_e estimation when the temperature varies significantly. (a) Drive cycle current. (b) Fluctuation of the battery core temperature. (c) Errors in R_e identification.

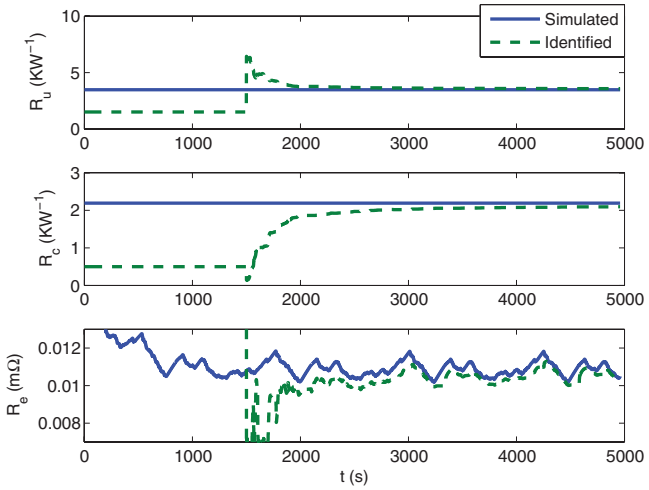

Fig. 14. Identification of temperature-dependent internal resistance by the least square algorithm with nonuniform forgetting factors.

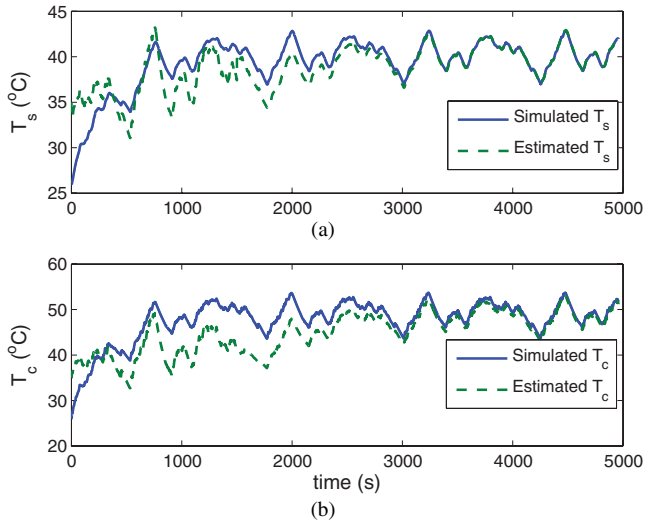

Fig. 15. Adaptive estimation of battery with temperature-dependent internal resistance by forgetting factors. (a) Estimation of surface temperature T_s. (b) Estimation of core temperature T_c.

where η_1 is the forgetting factor associated with α (and hence R_e).

Simulation is conducted with $\eta_1 = 0.25$, and the results of identification are shown in Fig. 14. It can be seen that that the identified R_e can follow the simulated varying R_e after the recursive least squares online identification with forgetting factors is activated at 1500 s. As shown in Fig. 15, the adaptive observer, taking the structure in (19) and parameters identified online (now R_e varying as shown in the bottom plot of Fig. 14), can estimate the battery core temperature T_c accurately after the identified R_e converges to the simulated R_e at around 3700 s.

VIII. Degradation Detection by Monitoring Growth in Internal Resistance

The recursive least square algorithm with forgetting factors can also track the long-term growth of the internal resistance, which can be used as an indication for the SOH of the battery.

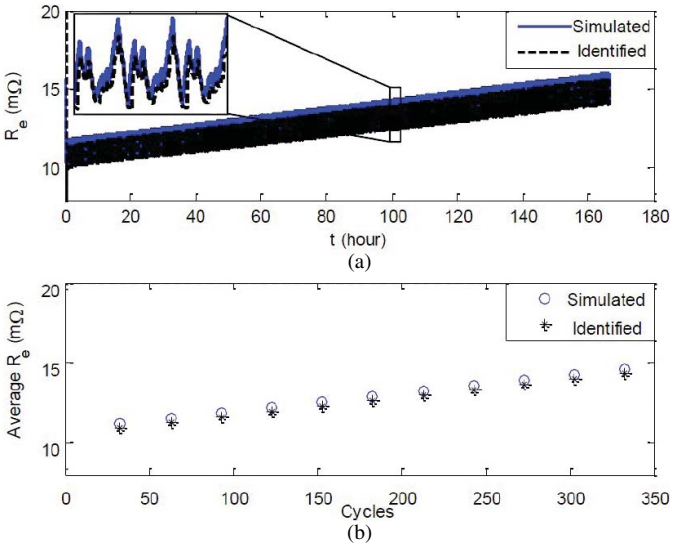

Fig. 16. Simulated identification of internal resistance subject to degradation. (a) Identification of R_e with both short-term and long-term variation. b) Simulated and identified cycle-average R_e.

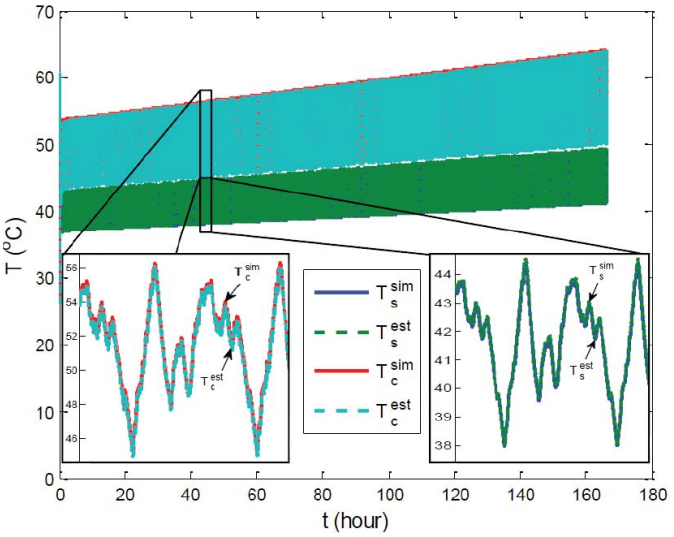

Fig. 17. Adaptive estimation of battery subject to degradation.

The growth of the internal resistance due to degradation is a process that occurs slowly over the battery lifetime. The internal resistance might increase substantially over hundreds of cycles or days according to [12]–[14].

In this paper, the growth in internal resistance due to degradation is simulated and used to test the capability of the identification algorithm to detect the slow increase of the resistance. The internal resistance R_e, originally a function of the core temperature T_c, is now augmented with a term, which is linearly increasing over time. The drive cycle used for simulation is the same as shown in the upper plot of Fig. 13, but is repeated for 350 times and the rate of growth in internal resistance is set at 0.14%/cycle. Although not modeled here, the rate of degradation may also increase with the temperature according to [12]–[14].

The results of the online identification are shown in Fig. 16. It can been seen from Fig. 16 that the simulated internal

resistance gradually increases over time while still subject to short-term variation due to the fluctuation of the battery core temperature. The identified R_e follows both the long-term and short-term variation of the simulated one with a small delay as shown in the inset of Fig. 16. In real vehicle application, since R_e is varying all the time, it is difficult to evaluate SOH by the instantaneous value of R_e and the averaged R_e might be a better choice instead. The mean value of R_e for each UAC cycle is plotted in the lower half of Fig. 16. It is noted that the averaged R_e can capture the long-term increase of the internal resistance and the identified value is a good estimation of the real one.

The adaptive monitoring of the temperatures is also shown in Fig. 17. It is noted that as the internal resistance of the battery grows, the temperatures will also be elevated due to the increase of the heat generated. Since the observer is updated with the identified R_e in real time, it estimates both the core and the surface temperatures with high accuracy.

IX. Conclusion

The core temperature of a lithium ion battery, which is usually not measurable, is of great importance to the onboard BMS, especially when the batteries are subject to drive cycles with high C-rate. The core temperature can be estimated by a two states thermal model, and the parameters of the models are critical for the accuracy of the estimation. In this paper, an online parameter identification scheme based on least square algorithm was designed for a cylindrical lithium ion battery thermal model. The online identification scheme can automatically identify model parameters based on the commonly available onboard signals. The updated parameters were then used to predict the unmeasured core temperature using a model-based observer as shown with an A123 26 650 lithium iron phosphate battery.

When the internal resistance of the battery is temperature-dependent, which is a more realistic situation, the least square algorithm was augmented with nonuniform forgetting factors. The algorithm with forgetting factors cannot only track the time-varying internal resistance, but also guarantee unbiased identification of the remaining constant parameters. The online parameterization also shows the capability to track the long-term variation of the internal resistance due to aging or degradation/abuse. The growth in internal resistance can be used for the SOH monitoring of the batteries. The methodology developed has been verified with simulations and is to be validated with experiments in the immediate future.

Applications, such as HEV, BEV, and PHEV, usually have hundreds, or even thousands, of battery cells in series to meet their high power and energy requirements. Hence the vehicle level battery thermal management will be performed on a module basis, instead of on a cell basis. The single cell thermal model used in this paper can be scaled up to a pack model by considering cell-to-cell thermal interaction, and the parameterization methodology and the adaptive observer design will be investigated for the pack level model. Initial results of this paper can be found in [22].

References

[1] C. Y. Wang and V. Srinivasan, "Computational battery dynamics (CBD)—electrochemical/thermal coupled modeling and multi-scale modeling," *J. Power Sour.*, vol. 110, no. 2, pp. 364–376, 2002.

[2] S. A. Hallaj, H. Maleki, J. Hong, and J. Selman, "Thermal modeling and design considerations of lithium-ion batteries," *J. Power Sour.*, vol. 83, nos. 1–2, pp. 1–8, 1999.

[3] H. Maleki and A. K. Shamsuri, "Thermal analysis and modeling of a notebook computer battery," *J. Power Sour.*, vol. 115, no. 1, pp. 131–136, 2003.

[4] W. B. Gu and C. Y. Wang, "Thermal-electrochemical modeling of battery systems," *J. Electrochem. Soc.*, vol. 147, no. 8, pp. 2910–2922, 2000.

[5] R. Mahamud and C. Park, "Reciprocating airflow for Li-ion battery thermal management to improve temperature uniformity," *J. Power Sour.*, vol. 196, no. 13, pp. 5685–5696, 2011.

[6] K. Smith and C.-Y. Wang, "Power and thermal characterization of a lithium-ion battery pack for hybrid-electric vehicles," *J. Power Sour.*, vol. 160, no. 1, pp. 662–673, 2006.

[7] D. Bernardi, E. Pawlikowski, and J. Newman, "A general energy balance for battery systems," *J. Electrochem. Soc.*, vol. 132, no. 1, pp. 5–12, 1985.

[8] C. Forgez, D. V. Do, G. Friedrich, M. Morcrette, and C. Delacourt, "Thermal modeling of a cylindrical $LiFePO_4$/graphite lithium-ion battery," *J. Power Sour.*, vol. 195, no. 9, pp. 2961–2968, 2010.

[9] C. W. Park and A. K. Jaura, "Dynamic thermal model of Li-ion battery for predictive behavior in hybrid and fuel cell vehicles," in *Proc. SAE Congr.*, 2003, no. 2003-01-2286, pp. 1835–1842.

[10] K. Smith, G.-H. Kim, E. Darcy, and A. Pesaran, "Thermal/electrical modeling for abuse-tolerant design of lithium ion modules," *Int. J. Energy Res.*, vol. 34, no. 2, pp. 204–215, 2009.

[11] Y. Hu, S. Yurkovich, Y. Guezennec, and B. Yurkovich, "Electro-thermal battery model identification for automotive applications," *J. Power Sour.*, vol. 196, no. 1, pp. 448–457, 2011.

[12] T. Yoshida, M. Takahashi, S. Morikawa, C. Ihara, H. Katsukawa, T. Shiratsuchi, and J. I. Yamakic, "Degradation mechanism and life prediction of lithium-ion batteries," *J. Electrochem. Soc.*, vol. 153, no. 3, pp. A576–A582, 2006.

[13] Z. Li, L. Lu, M. Ouyang, and Y. Xiao, "Modeling the capacity degradation of $LiFePO_4$/graphite batteries based on stress coupling analysis," *J. Power Sour.*, vol. 196, no. 22, pp. 9757–9766, 2011.

[14] J. Hall, A. Schoen, A. Powers, P. Liu, and K. Kirby, "Resistance growth in lithium ion satellite cells. I. Non destructive data analyses," in *Proc. 208th ECS Meeting*, Los Angeles, CA, Oct. 2005, p. 1.

[15] A. P. Schmidt, M. Bitzer, and L. Guzzella, "Experiment-driven electrochemical modeling and systematic parameterization for a lithium-ion battery cell," *J. Power Sour.*, vol. 195, no. 15, pp. 5071–5080, 2010.

[16] M. Verbrugge and E. Tate, "Adaptive state of charge algorithm for nickel metal hydride batteries including hysteresis phenomena," *J. Power Sour.*, vol. 126, nos. 1–2, pp. 236–249, 2004.

[17] B. Saha, K. Goebel, S. Poll, and J. Christophersen, "Prognostics methods for battery health monitoring using a Bayesian framework," *IEEE Trans. Instrum. Meas.*, vol. 58, no. 2, pp. 291–296, Feb. 2009.

[18] H. E. Perez, J. B. Siegel, X. Lin, A. G. Stefanopoulou, Y. Ding, and M. P. Castanier, "Parameterization and validation of an integrated electro-thermal LFP battery model," in *Proc. ASME Dynam. Syst. Control Conf.*, 2012, pp. 1–10.

[19] X. Lin, H. E. Perez, J. B. Siegel, A. G. Stefanopoulou, Y. Li, and R. D. Anderson, "Quadruple adaptive observer of the core temperature in cylindrical Li-ion batteries and their health monitoring," in *Proc. Amer. Control Conf.*, 2012, pp. 1–6.

[20] P. A. Ioannou and J. Sun, *Robust Adaptive Control*. Englewood Cliffs, NJ: Prentice-Hall, 1996.

[21] A. Zukauskas, "Heat transfer from tubes in crossflow," *Adv. Heat Transfer*, vol. 8, pp. 93–160, 1972.

[22] X. Lin, H. E. Perez, J. B. Siegel, A. G. Stefanopoulou, Y. Ding, and M. P. Castanier, "Parameterization and observability analysis of scalable battery clusters for onboard thermal management," *J. Oil Gas Sci. Technol.*, 2012, to be published.

[23] T.-K. Lee, Y. Kim, A. G. Stefanopoulou, and Z. Filipi, "Hybrid electric vehicle supervisory control design reflecting estimated lithium-ion battery electrochemical dynamics," in *Proc. Amer. Control Conf.*, 2011, pp. 388–395.

[24] J. Windsor, L. Silverberg, and G. Lee, "Convergence rate analysis of a multivariable recursive least squares parameter estimator," in *Proc. Amer. Control Conf.*, 1994, pp. 465–469.

[25] A. Astrom and B. Wittenmark, *Adaptive Control*. Reading, MA: Addison-Wesley, 1989.
[26] R. Williams and D. Lawrence, *Linear State-Space Control Systems*. New York: Wiley, 2007.
[27] R. E. Kalman, "A new approach to linear filtering and prediction problems," *Trans. ASME J. Basic Eng.*, vol. 82, pp. 35–45, 1960.

Xinfan Lin received the B.S. and M.S. degrees in automotive engineering from Tsinghua University, Beijing, China, in 2007 and 2009, respectively. He is currently pursuing the Ph.D. degree with the Department of Mechanical Engineering, University of Michigan, Ann Arbor.

His current research interests include thermal modeling, identification and estimation of lithium ion batteries, and detection of imbalance in battery strings.

Hector E. Perez received the B.S. degree in mechanical engineering from California State University, Northridge, in 2010. He is currently pursuing the M.S.E. degree in mechanical engineering with the University of Michigan, Ann Arbor.

He is currently a Graduate Student Research Assistant of mechanical engineering with the University of Michigan. His current research interests include experimental validation of electrothermal lithium ion battery models.

Mr. Perez was a recipient of the GEM Fellowship sponsored by the Oak Ridge National Laboratory and the University of Michigan.

Jason B. Siegel received the B.S., M.S., and Ph.D. degrees from the University of Michigan, Ann Arbor, in 2004, 2006, and 2010 respectively.

He is currently a Postdoctoral Research Fellow with the Powertrain Control Laboratory, University of Michigan. His current research interests include modeling and control of alternative energy storage and conversion systems for automotive applications.

Anna G. Stefanopoulou (F'09) is a Professor of mechanical engineering and the Director of the Automotive Research Center, University of Michigan, Ann Arbor. From 1998 to 2000, she was an Assistant Professor with the University of California, Santa Barbara. From 1996 to 1997, she was a Technical Specialist with Ford Motor Company. She has authored or co-authored more than 200 papers and a book on estimation and control of internal combustion engines and electrochemical processes such as fuel cells and batteries. She holds nine U.S. patents.

Prof. Stefanopoulou is a Fellow of the ASME. She was a recipient of four Best Paper Awards.

Yonghua Li received the Ph.D. degree in control theory and applications from the Beijing University of Aeronautics and Astronautics, Beijing, China.

He has intensive experience in academia and industry. He is currently a Research Engineer with the Research and Advanced Engineering Division, Ford Motor Company, Dearborn, MI. His current research interests include supervisory control of discrete event systems, automotive engine control, hybrid vehicle control, and automotive traction battery management systems. He has authored or co-authored a number of papers in journals and conferences. He holds several U.S. patents.

R. Dyche Anderson received the B.S. ChE. degree from Michigan Technological University, Houghton, and the M.S. degree in chemical engineering from New Mexico State University, Las Cruces.

He is currently a Technical Expert of Battery Controls with Ford Motor Company, Dearborn, MI. He is involved in leading the Advanced Battery Controls and Systems Group, Ford Research and Advanced Engineering Division. He has 25 years of experience in batteries, battery controls, and battery systems at both Ford and the Naval Surface Warfare Center, Crane, IN. He has researched a wide variety of battery chemistries, including primary, secondary, and reserve systems. He has conducted research on product development, supervised development of batteries, battery systems, and battery controls and has delivered batteries, battery controls, and/or battery systems for automotive, missile, and other applications. He is involved in the development of a training course on internal battery controls used globally with Ford Motor Company. He has authored or co-authored numerous papers. He holds two patents on battery controls technology.

Yi Ding is currently an Electrical Engineer with Ground Vehicle Power & Mobility, U.S. Army Tank Automotive Research, Development, and Engineering Center, Warren, MI. He is involved in monitoring energy storage research and development status and assisting the Energy Storage Team in monitoring technical progress of R&D projects. He has more than 20 years of experience in battery research and development and project management.

Matthew P. Castanier received the B.S., M.S., and Ph.D. degrees from the University of Michigan, Ann Arbor, in 1989, 1992, and 1995, respectively.

He is currently a Research Mechanical Engineer with the U.S. Army Tank Automotive Research, Development, and Engineering Center, where he has been since 2008. He was a Research Faculty Member for 12 years in the Department of Mechanical Engineering, University of Michigan. His current research interests include reduced-order modeling of ground vehicle structures, modeling and simulation of automotive energy storage systems, and multidisciplinary design optimization. He has authored or co-authored more than 30 articles in archival journals and over 75 papers in refereed conference proceedings.